Journal of Pathology
J Pathol 2012; **228:** 45–55
Published online 6 June 2012 in Wiley Online Library
(wileyonlinelibrary.com) DOI: 10.1002/path.4033

ORIGINAL PAPER

The CREB–Smad6–Runx2 axis contributes to the impaired osteogenesis potential of bone marrow stromal cells in fibrous dysplasia of bone

Qi-Ming Fan,[1] Bing Yue,[1] Zhen-Yu Bian,[1] Wen-Ting Xu,[1] Bing Tu,[1] Ke-Rong Dai,[1] Gang Li[2]* and Ting-Ting Tang[1]*

[1] *Shanghai Key Laboratory of Orthopaedic Implants, Department of Orthopaedic Surgery, Shanghai Ninth People's Hospital, Shanghai JiaoTong University School of Medicine, Shanghai, People's Republic of China*
[2] *Department of Orthopaedics and Traumatology, Chinese University of Hong Kong, People's Republic of China*

**Correspondence to: Ting-Ting Tang, Shanghai Key Laboratory of Orthopaedic Implants, Department of Orthopaedic Surgery, Shanghai Ninth People's Hospital, Shanghai JiaoTong University School of Medicine, 639 Zhizaoju Road, Shanghai 200011, People's Republic of China.*
e-mail: tingtingtang@hotmail.com or Gang Li, Department of Orthopaedics & Traumatology, The Chinese University of Hong Kong, Room 904, 9/F, Li Ka Shing Institute of Health Sciences, Prince of Wales Hospital, Shatin, Hong Kong, SAR, People's Republic of China. e-mail: gangli@ort.cuhk.edu.hk

Abstract

Fibrous dysplasia (FD) is characterized by the replacement of normal bone with abnormal fibro-osseous tissue. This disorder is due to activating missense mutations in the *GNAS* gene and resultant over-production of cAMP. However, the signalling pathways that contribute to FD pathogenesis remain unknown. In the current study, bone marrow stromal cells (BMSCs) carrying *GNAS* R201H mutation were isolated from lesion site of FD patients. cAMP accumulation, enhanced proliferation and impaired osteogenesis potential were observed. Two cell models, BMSCs treated with excess exogenous cAMP and BMSCs infected with lentivirus GNAS R201H, were established to model the pathological conditions of FD and used to investigate its pathogenesis. The results suggest that the CREB-Smad6-Runx2 axis is involved in osteogenesis dysfunction of BMSCs with the FD phenotype. We confirmed the results in FD lesion-derived BMSCs and observed that the impaired osteogenesis potential of BMSCs infected with lentivirus *GNAS* (R201H) was recovered *in vitro* through modulation of the CREB-Smad6-Runx2 axis. This study provides useful insight into the signalling pathways involved in the FD phenotype and facilitates dissection of the molecular pathogenesis of FD and testing of novel therapies.

Keywords: fibrous dysplasia; GNAS; cAMP; CREB; Smad6; Runx2

Received 6 January 2012; Revised 9 March 2012; Accepted 20 March 2012

No conflicts of interest were declared.

Introduction

Fibrous dysplasia (FD) is a severe disorder that occurs as either a purely skeletal disease [1] or in conjunction with endocrinopathies and skin hyperpigmentation as part of McCune–Albright syndrome (MAS; OMIM# 174 800) [2] or in conjunction with intramuscular myxoma as part of Mazabraud syndrome [3,4]. FD lesions develop as both bone and marrow are replaced with structurally disorganized and unsound bone and fibrotic tissues that are devoid of haematopoiesis and marrow adipocytes [5–9]. This abnormal pattern is rooted in the shared origin of osteoblasts, myelosupportive stroma and adipocytes as skeletal stem cells [also known as 'mesenchymal stem cells' within the bone marrow stromal cell (BMSC) population].

Activating missense mutations of *GNAS*, which encodes the α-subunit of stimulatory G (Gs) protein, underlie MAS-associated FD and most likely many types of non-MAS-associated FD [10–12]. Substitution of either Cys or His for Arg at position 201 in the Gsα-subunit leads to the loss of its GTPase activity resulting in increased activation of adenylyl cyclase (AC) and over-production of cAMP. This somatic mutation has been demonstrated in a variety of tissues from patients with MAS, including bone [11,13–17], and in samples from the monostotic form of FD [15,18,19]. Owing to these mutations, both the differentiation of BMSCs and the function of mature osteoblasts are severely altered, leading to replacement of normal bone/marrow with abnormal bone/marrow, which together comprise a single FD lesion [20].

The FD BMSC population is a mixture of normal and mutant cells. When transplanted *in vivo*, clones with a normal genotype formed a normal ossicle, as expected [21]. Surprisingly, when clones with a mutant genotype were transplanted, the mutant cells did not survive and formed a 'non-ossicle' [21]. These data indicate that not only are the patients somatic mosaics, but the lesions are mosaics as well.

Here we sought to elucidate the molecular mechanisms underlying how *GNAS* mutation leads to an osteogenesis disorder of BMSCs.

Materials and methods

Isolation, culture and osteogenesis induction of BMSCs from FD lesions

Under an approved protocol for the use of human subjects in research, FD lesions were harvested from three donors (donor 1, aged 17 years, female, humeral, *GNAS* R201H; donor 2, aged 20 years, male, radius, *GNAS* R201H; and donor 3, aged 19 years, female, humeral, *GNAS* R201H). The FD lesions were rinsed with α-MEM (Gibco) containing 10% fetal bovine serum (FBS; Hyclone) and antibiotics and then the liberated cells were incubated in 5% CO_2 at 37 °C. The medium was changed twice a week until confluence was achieved. As a control, normal BMSCs were isolated from bone marrows of three healthy donors (aged 20–26 years).

To induce osteogenesis, we exposed BMSCs to rhBMP2 (200 ng/ml; R&D). The medium was changed every 3 days. The expression levels of collagen I, OPN and OC were analysed at 2, 3 and 4 weeks after induction, respectively. Calcium deposition was measured through alizarin red staining 4 weeks after induction.

cAMP treatment

To investigate the effect of excess cAMP on osteogenesis of BMSCs, we exposed confluent BMSCs to medium containing BMP-2 and 2 mM dibutyryl–cAMP (Sigma, St. Louis, MO, USA). The medium was changed every 3 days.

cAMP measurement

Cells were plated in 24-well plates and incubated for 1 h in serum-free medium in the presence of 1 mM IBMX (Sigma) after reaching confluence. cAMP was extracted by 0.1 N HCl and kept frozen before measurement using the Cyclic AMP EIA Kit (Cayman), according to the manufacturer's instructions.

Mutation analysis

An approximately 300 bp cDNA sequence of *GNAS* (NCBI Gene ID 2778) was chosen as the target for PCR amplification. The RT–PCR primer sequences used were as follows: wild-type, 5′-GACCTGCTTCGCTG G*CG-3′; R201H, 5′-GGACCTGCTTCGCTGG*C (A)-3′; R201C, 5′-CAGGACCTGCTTCGCTC*C (T)-3′ (where * denotes internal mismatching and parentheses denoting the base transition) and reverse, 5′-TCTTGCTTGTTGAGGAACAG-3′. A 270 bp sequence of *GNAS* containing the Arg201 codon was amplified from FD-derived BMSCs, using the following primers: 5′-TGACTATGTGCCGAGCGA-3′ (forward) and 5′-AACCATGATCTCTGTTATATAA-3′ (reverse). The product was purified using the QIAquick PCR Purification Kit (Qiagen) and cloned into the pMD19-T vector system (Takara). Fifty clones/sample were sequenced to assess the *GNAS* mutation status.

MTT assay

Briefly, 1×10^3 cells were seeded in a 96-well plate. At each indicated time point, MTT solution was added, and the plates were incubated for 3–4 h. Subsequently, DMSO (Sigma) was added and the plate was incubated for 5 min. The plates were then read at 570 nm, using an automated plate reader (Perkin-Elmer).

Real-time PCR

Total RNA was isolated using TRIzol reagent (Invitrogen). The real-time PCR conditions were as follows: 40 cycles of 94 °C for 10 s and 60 °C for 30 s. A melting stage was added to the end of the amplification procedure. β-Actin was used as the loading control. The primer sequences are listed in Table S1 (see Supporting information).

Lentivirus and adenovirus vectors

A lentivirus expression vector loading human *GNAS* coding sequence was purchased from Genecopoeia™ and subjected to *in vitro* point mutagenesis to replace CGT with CAT (R to H). Briefly, $1.3–1.5 \times 10^6$ 293T cells were plated in a 10 cm dish so that 70–80% confluence was obtained at the moment of transfection. The transfection complex was added directly to each dish. The cells were then incubated in a CO_2 incubator at 37 °C overnight. Pseudovirus-containing culture medium was collected 48 h post-transfection. Adenovirus–Runx2 and adenovirus–siRNA–Smad6 vectors were purchased from Invitrogen (China).

Luciferase reporter gene assay

Luciferase reporter vectors driven by the Smad6 (NCBI Gene ID 4091) promoter with or without the CRE were used for transfection. The phRL-SV40 vector (Promega) was used as the transfection efficiency control. Both firefly and *Renilla* luciferase activities were measured using a dual-luciferase reporter assay system (Promega).

Chromatin immunoprecipitation assay

Briefly, the cells were fixed with 1% formaldehyde, lysed in SDS lysis buffer and sonicated to shear DNA to an average fragment size of 300–400 bp. An anti-phospho-CREB antibody (Santa Cruz Biotechnology) was then added. After overnight incubation at 4 °C, immune complexes were collected using salmon sperm DNA/protein agarose −50% slurry. Samples were extracted with elution buffer (1% SDS, 0.1 M $NaHCO_3$) and heated at 65 °C overnight to reverse crosslinking. The primer set was as follows: 5′-CTCCAGGGGCAGGAGCGGC-3′ (forward) and 5′-CGCCGGCCGGCCGGGCCCCCT-3′ (reverse).

Transplants

Briefly, BMSCs (passages 2–4, $1.5–6.0 \times 10^6$ cells) attached to β-tricalcium phosphate (TCP; Shanghai

Bio-lu Biomaterials Co. Ltd) were transplanted subcutaneously into the back of Balb/c mice under an institutionally approved protocol for the care and use of animals in research.

Statistical analysis

Statistical significance was calculated for two-sample comparisons using Student's *t*-test, and one-way ANOVA was used for multiple comparisons. Tukey's test was used to evaluate significant differences identified by ANOVA. $p < 0.05$ was defined as significant.

Results

Osteogenesis potential is impaired in BMSCs from FD lesions

We isolated BMSCs from excised FD lesions (Figure 1). The R201H mutation in *GNAS* was confirmed by allele-specific PCR and sequencing (Figure 2A). As expected, the cAMP levels were much higher in the FD-derived BMSCs than in the control (approximately four-fold greater) (Figure 2B). Enhanced proliferation was also observed in the FD-derived BMSCs compared to the control (Figure 2C).

We next investigated the *in vitro* osteogenesis potential of these BMSCs. BMP-2 (200 ng/ml) was employed to induce osteogenesis *in vitro* (see Supporting information, Figure S1). Expression of collagen I, OPN and OC and calcium deposition were not up-regulated in FD-derived BMSCs after treatment with BMP-2, suggesting that the responsiveness to BMP-2 induction was lower in FD-derived BMSCs compared to the control (Figure 2D, E). Following the assessment of *in vitro* osteogenesis, we explored the *in vivo* osteogenesis potential of FD-derived BMSCs. Less mature bone was observed in the pores of β-TCP loaded with FD-derived BMSCs, and most areas were occupied by fibroblastic tissues (Figure 2F). Mature bone was found in the scaffold loaded with normal BMSCs. Additionally, FD-like lesion could be reconstructed by injecting FD-derived BMSCs into the bone marrow cavity of nude mice (see Supporting information, Figure S2). These results suggested that the FD-derived BMSCs presented an impaired osteogenesis potential *in vitro* and *in vivo*.

Transfer of the FD phenotype to normal BMSCs by lentivirus infection and exogenous cAMP treatment

In the current study, we isolated several BMSC clones with mutated *GNAS* from FD patients (see Supporting information, Figure S3). However, these cells could not grow normally *in vitro*; therefore, we established two *in vitro* cell models that could mimic the pathological features of FD. The first was to stably transfer R201H *GNAS* into normal BMSCs. We constructed a lentivirus vector expressing mutated *GNAS* (R201H) (Figure 3A) and used it to infect normal BMSCs. After puromycin treatment, cell clones stably expressing mutated *GNAS* (R201H) were available (Figure 3B). The cAMP concentration was significantly higher in LV-R201H BMSCs than in control cells (Figure 3C).

Another cell model was employed in the current study: normal BMSCs treated with exogenous 2 mM cAMP (see Supporting information, Figure S1). These two cell models were induced to mimic the osteogenesis induced with BMP-2 *in vitro* and the effects of the *GNAS* R201H mutation and excess cAMP on the osteogenesis of BMSCs were investigated. Unlike FD-derived BMSCs, there was no difference in collagen I mRNA expression levels in LV-R201H BMSCs and cAMP-treated BMSCs compared to control cells treated with BMP-2. In contrast, OPN and especially OC were not up-regulated by BMP-2 in LV-R201H BMSCs and cAMP-treated BMSCs compared to control cells treated with BMP-2 (Figure 3D). In addition, the results of alizarin red staining supported these data (Figure 3E, F). IBMX, a competitive non-selective phosphodiesterase inhibitor that raises intracellular cAMP levels, decreased calcium deposition in synergy with the *GNAS* mutation (Figure 3F).

Runx2 down-regulation and Smad6 up-regulation in BMSCs with the FD phenotype

We screened three key transcription factors in osteogenesis, Runx2, Msx2 and Osx, by exposing normal BMSCs to BMP-2 and excess cAMP and quantifying their mRNA abundance. *Runx2* and *Osx* mRNA levels were not up-regulated and *Msx2* expression was up-regulated in response to BMP-2 and excess cAMP treatment, suggesting that *Runx2* and *Osx* might

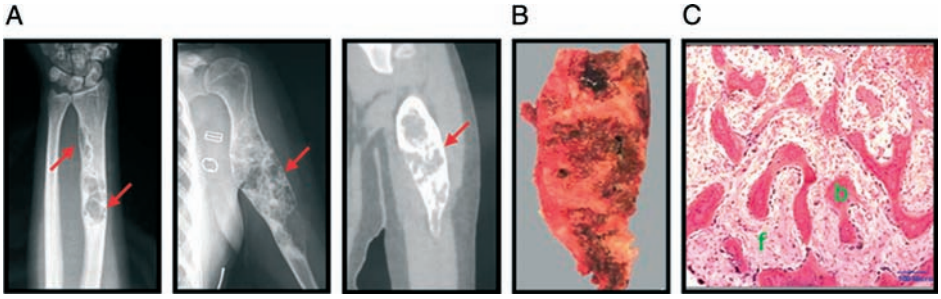

Figure 1. Fibrous dysplasia (FD). (A) Radiographic examination. FD lesions were observed in the mid-humeral shaft and distal radius (red arrows). (B) Fibrotic lesion subjected to surgical resection. (C) Haematoxylin and eosin (H&E) staining of the excised FD lesion; b, bone tissue; f, fibrotic tissue.

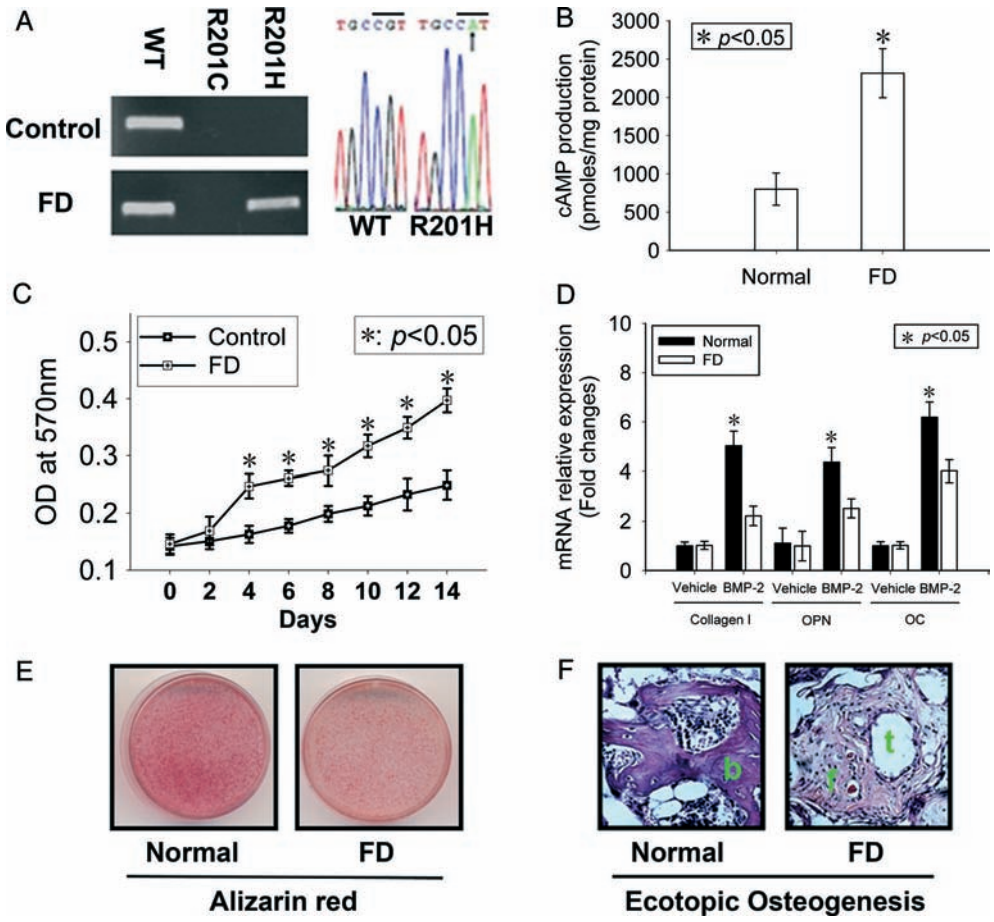

Figure 2. Features of bone marrow stromal cells (BMSCs) from the fibrous dysplasia (FD) lesions. BMSCs were isolated from excised FD lesions of the patients. Normal BMSCs from healthy donors were used as controls. (A) Allele-specific PCR using primers for the R201H and R201C mutations and sequencing after cloning into the T vector were employed to analyse the *GNAS* mutations; black arrow indicates mutation of a nucleotide. (B) cAMP levels; $^{**}p < 0.01$, FD versus control. (C) MTT assay; $^{*}p < 0.05$, FD versus control. (D) Collagen I (2 weeks after BMP-2 induction), osteopontin (*OPN*; 3 weeks) and osteocalcin (*OC*; 4 weeks) mRNA expression by real-time PCR. The results are expressed as fold changes of FD cells relative to the control; $^{*}p < 0.05$, FD versus control. (E) Alizarin red staining assay. (F) *In vivo* ectopic osteogenesis assay; BMSCs from healthy donors and FD lesion sites were combined with β-TCP scaffolds and transplanted subcutaneously into the backs of nude mice ($n = 8$ in each group). Eight weeks later, transplants were harvested and subjected to H&E staining. All numerical data are presented as mean ± SD. These data were from at least three independent experiments.

be the targets of cAMP (see Supporting information, Figure S4). BMP-2 has been shown to regulate Osx through Msx2 and Runx2 during osteogenesis [23]. Therefore, we identified Runx2 as a potential target in the cAMP-dependent pathway.

At day 1 after BMP-2 treatment, mRNA and protein expression levels of Runx2 were investigated. Runx2 was down-regulated in LV-R201H BMSCs and cAMP-treated BMSCs compared to control cells treated with BMP-2. Moreover, in the presence of IBMX, Runx2 was down-regulated more significantly in LV-R201H BMSCs than in the absence of IBMX, suggesting that excess cAMP played an important role in the attenuation of Runx2 responsiveness to BMP-2 induction in BMSCs with the FD phenotype (Figure 4A, B).

We then asked whether excess cAMP could directly result in Runx2 down-regulation. The mRNA expression of *Runx2* was assayed 0–48 h after the addition of BMP-2 and cAMP to normal BMSCs. There was no difference in *Runx2* expression between 3 and 6 h. Runx2 was down-regulated until 12 h (Figure 4C), suggesting that excess cAMP does not directly result in *Runx2* down-regulation, but requires some signalling factors to mediate it. Thus, the expression levels of several members in the BMP-Smads signalling pathway were investigated in response to excess cAMP. A remarkable up-regulation of Smad6, an inhibitor of the BMP–Smads signalling pathway [24], was observed in normal BMSCs treated with BMP-2 and exogenous cAMP (Figure 4D, E). However, Smad6 up-regulation in LV-R201H BMSCs was less significant than in cAMP-treated BMSCs. In the presence of IBMX, the expression level of Smad6 was slightly up-regulated than in the absence of IBMX (Figure 4E).

We then hypothesized that Runx2 down-regulation might be mediated by Smad6 up-regulation in BMSCs with the FD phenotype. To test this hypothesis, we silenced Smad6 expression by siRNA and quantified Runx2 expression. As expected, Runx2 expression, which was down-regulated in LV-R201H BMSCs and cAMP-treated BMSCs, was effectively recovered in response to Smad6 silencing (Figure 4F).

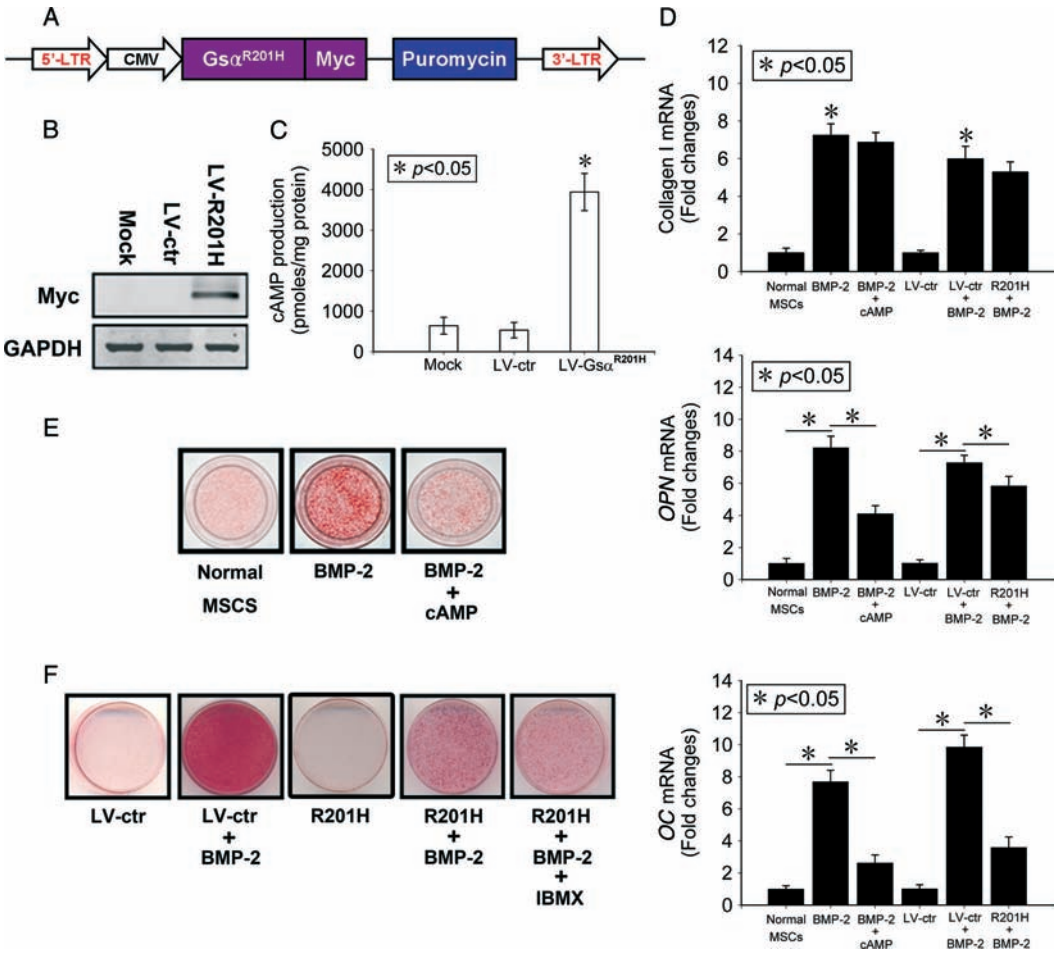

Figure 3. Transfer of the FD phenotype to BMSCs by lentivirus transduction and exogenous excess cAMP treatment. (A) Map of the lentivirus vector loading $Gs\alpha^{R201H}$. (B) Western blot: an anti-myc antibody was used, and mock- and LV-ctr-treated cells were used as controls. GAPDH was used as the loading control. (C) cAMP levels; $^*p < 0.05$, LV-$Gs\alpha^{R201H}$ versus mock and LV-ctr. (D) Collagen I (2 weeks after BMP2 induction), osteopontin (*OPN*, 3 weeks) and osteocalcin (*OC*, 4 weeks) mRNA expression by real-time PCR; the results are expressed as fold changes of every treatment group relative to controls; $^*p < 0.05$. (E, F) Alizarin red staining; this assay was performed 4 weeks after induction of osteogenesis by BMP-2. All numerical data are presented as mean ± SD. These data were from at least three independent experiments.

CREB activates Smad6 expression through binding to the CRE in the Smad6 promoter in BMSCs with the FD phenotype

We further screened the Smad6 promoter region and observed that there was a putative cAMP responsive element (CRE) in the −1006 bp to −995 bp region. We cloned the −1280 to +65 bp region into a luciferase reporter vector and then constructed 5′ deletion mutants with and without this CRE. A luciferase reporter assay showed that cAMP could increase the activity of the Smad6 promoter containing the CRE (−1280 to +65 bp) in cAMP-treated BMSCs, and deletion of the CRE decreased the luciferase activity significantly. In LV-R201H BMSCs, the CRE had no effect on the activity of the Smad6 promoter containing the CRE (−1280 to +65 bp) in the absence of IBMX. However, in the presence of IBMX, deletion of the CRE decreased the luciferase activity significantly (Figure 5A), highlighting the role of cAMP in Smad6 up-regulation driven by the CRE in BMSCs with the FD phenotype.

The CRE activates transcription of target genes through recruitment of the CRE binding protein (CREB). We co-transfected a dominant-negative CREB (DN CREB) expression vector (unable to bind the CRE) and the −1280/+65 CRE-containing luciferase construct into LV-R201H BMSCs and cAMP-treated BMSCs. The luciferase activity of the −1280/+65 construct was remarkably up-regulated in cAMP-treated BMSCs and LV-R201H BMSCs treated with IBMX and was down-regulated significantly in response to DN CREB (Figure 5B), suggesting the possible involvement of CREB in Smad6 expression in BMSCs with the FD phenotype.

A chromatin immunoprecipitation assay using primers for the −1041 to −827 bp region flanking the CRE in the Smad6 promoter was performed to confirm the binding of CREB to the CRE in the Smad6 promoter region. In cAMP-treated BMSCs and LV-R201H BMSCs treated with IBMX, CREB exhibited a strong binding affinity to the CRE (Figure 5C). However, binding was not observed in DN CREB, indicating that CREB is involved in Smad6 up-regulation

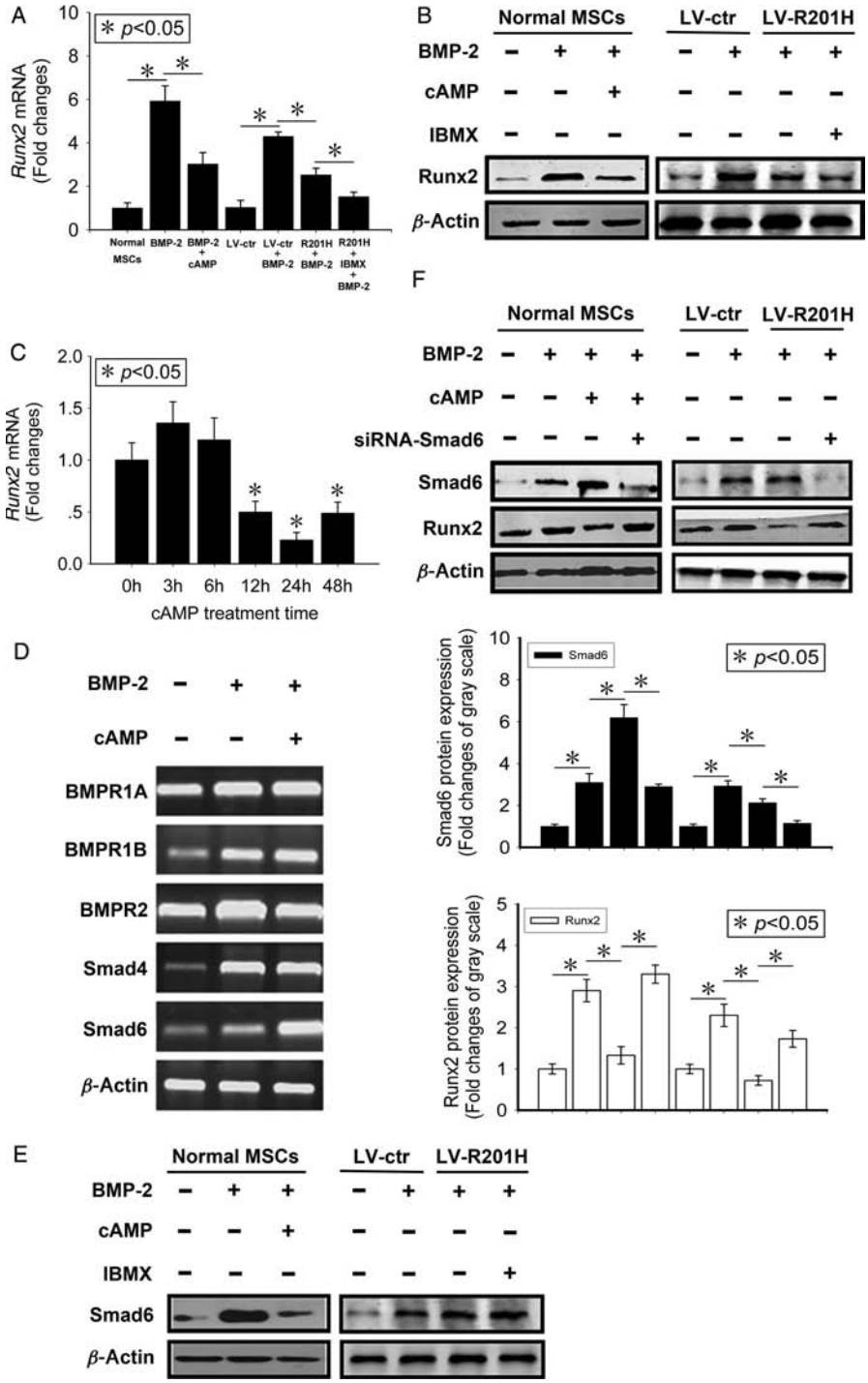

Figure 4. Runx2 down-regulation and Smad6 up-regulation in the FD phenotype of BMSCs. (A): Real-time PCR for *Runx2* mRNA expression performed in BMSCs with the FD phenotype by lentivirus transduction and exogenous cAMP treatment 48 h after BMP-2 addition; the results are expressed as fold changes of every treatment group relative to controls; $^{*}p < 0.05$. (B) Western blot for Runx2 protein expression; β-actin was used as the loading control. (C) Real-time PCR for *Runx2* mRNA expression in BMSCs treated with excess cAMP at the indicated time points; the results are expressed as fold changes of other groups relative to 0 h; $^{*}p < 0.05$ versus 0 h. (D) mRNA expression profile (RT–PCR) of signalling molecules in the BMP–Smads signalling pathway 24 h after induction of osteogenesis by BMP-2; β-actin was used as the loading control. (E) Western blot for Smad6 protein expression in BMSCs with the FD phenotype by lentivirus transduction and exogenous cAMP treatment 24 h after induction of osteogenesis by BMP-2. (F) Runx2 protein expression 2 days after BMP-2 induction in response to knockdown of Smad6 by transient transfection of adenovirus-siRNA-Smad6; β-actin was used as the loading control. Relative protein expression of Smad6 and Runx2 was analysed using QuantityOne™ software; $^{*}p < 0.05$. All numerical data are presented as mean ± SD. These data were from at least three independent experiments.

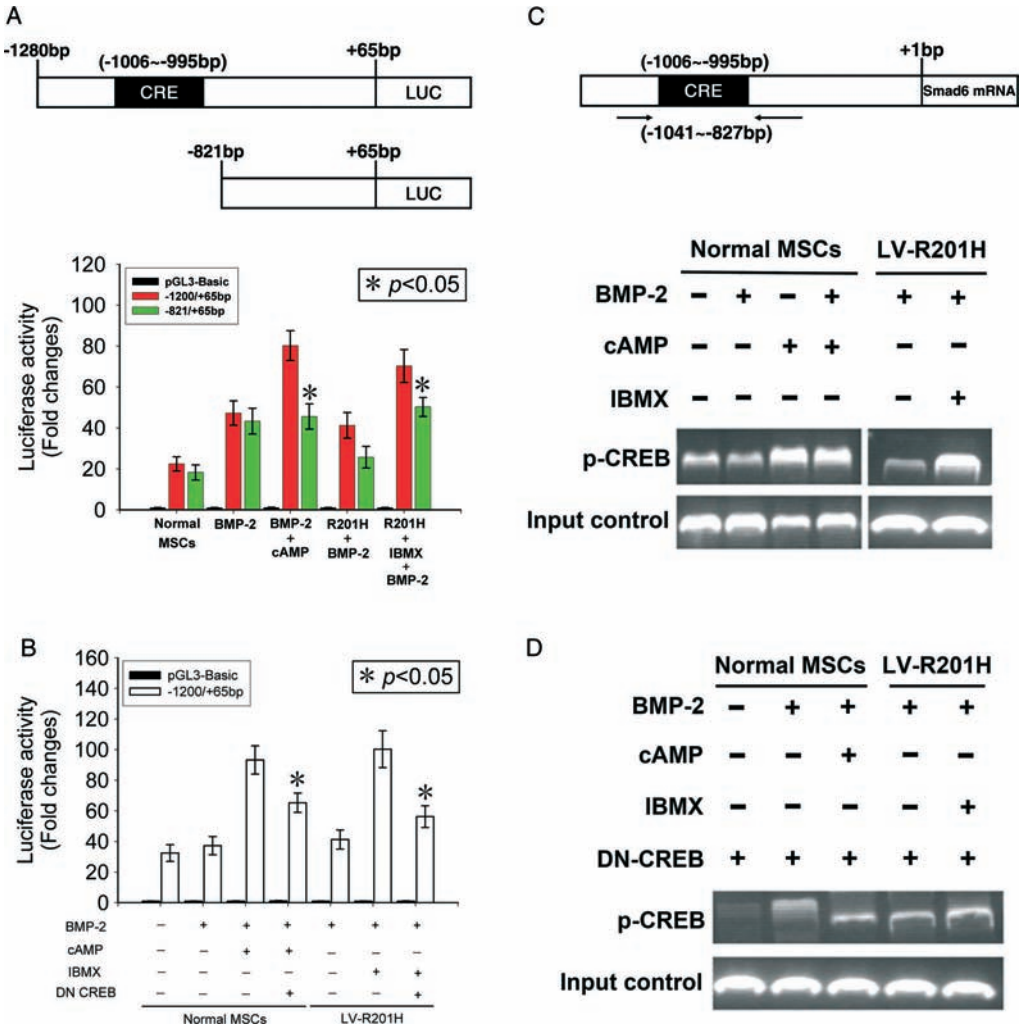

Figure 5. CREB activates Smad6 expression through binding to the CRE in the Smad6 promoter in BMSCs with the FD phenotype. (A) Luciferase reporter gene assay using 5′ deletion mutants with and without the CRE in the Smad6 promoter region; the results are expressed as fold changes of every construct relative to pGL3-basic; $^*p < 0.05$, −821/+65 bp versus −1200/+65 bp. (B) The effect of dominant-negative CREB (DN CREB) on the luciferase activity of 5′ deletion mutants with and without the CRE in the Smad6 promoter region; the results are expressed as fold changes of −1200/+65 bp construct relative to pGL3-basic; $^*p < 0.05$, −1200/+65 bp in (+)BMP-2(+)cAMP(+)DN CREB versus −1200/+65 bp in (+)BMP-2(+)cAMP, −1200/+65 bp in (+)BMP-2(+)IBMX(+)DN CREB versus −1200/+65 bp in (+)BMP-2(+)IBMX. (C) Chromatin immunoprecipitation using primers for the −1041 bp to −827 bp region of the Smad6 promoter in BMSCs with the FD phenotype. (D) ChIP using DN CREB. All numerical data are presented as mean ± SD. These data were from at least three independent experiments.

in LV-R201H BMSCs and cAMP-treated BMSCs (Figure 5D).

In vitro recovery of the impaired osteogenesis potential of LV-R201H BMSCs through modulation of Runx2 and Smad6

We wanted to investigate whether the CREB–Smad6–Runx2 axis would exert the same effect in FD-derived BMSCs. Runx2 and Smad6 expression and the binding of CREB to CRE in the Smad6 promoter region were investigated during osteogenesis of FD-derived BMSCs. Compared with the control treated by BMP-2, Runx2 was down-regulated, Smad6 was up-regulated and the CREB showed an enhanced binding ability on CRE in the Smad6 promoter (Figure 6A, B).

We further investigated the possibility of *in vitro* recovery of the impaired osteogenesis potential of LV-R201H BMSCs through modulation of this axis. Two adenovirus vectors, Adv-Runx2 and Adv-siRNA-Smad6, were constructed to over-express Runx2 and silence Smad6 in LV-R201H BMSCs. We observed that the *in vitro* osteogenesis potential, marked by collagen I (Figure 6C), OPN (Figure 6D), OC (Figure 6E) and calcium deposition (Figure 6F), which were impaired in the FD phenotype, was recovered in response to Runx2 over-expression or Smad6 knockdown. Moreover, the impaired osteogenesis of cAMP-treated BMSCs could be recovered by Runx2 over-expression (see Supporting information, Figure S5).

Discussion

The pathogenesis of FD has been an area of intense research interest. Breakthroughs were made in 1991

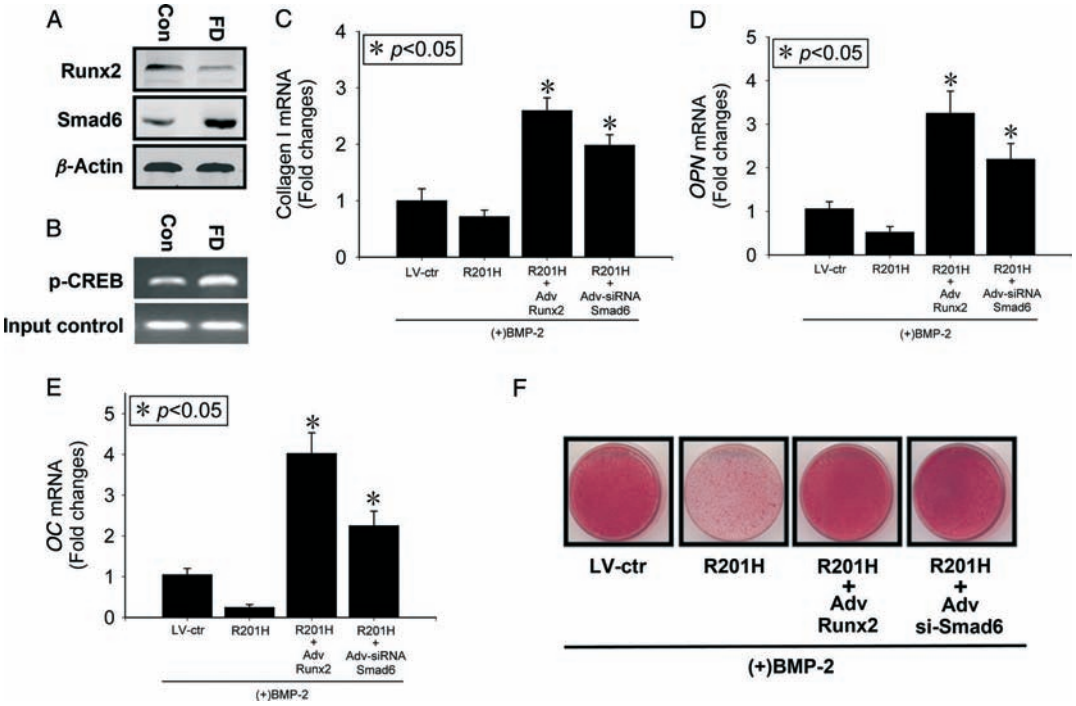

Figure 6. *In vitro* recovery of the impaired osteogenesis potential of LV-R201H BMSCs through modulation of Runx2 and Smad6. (A) Western blot analysis of Smad6 (1 day after BMP2 induction) and Runx2 (2 days after induction) protein expression in BMSCs from FD lesions. (B) Chromatin immunoprecipitation using primers for the −1041 bp to −827 bp region of the Smad6 promoter in BMSCs from the FD lesion sites 1 day after BMP-2 induction. Real-time PCR for mRNA expression of collagen I (C), *OPN* (D) and *OC* (E) and alizarin red staining for calcium deposition (F) in BMSCs with the FD phenotype by lentivirus transduction were performed in response to Runx2 over-expression and Smad6 knockdown by an adenovirus vector; the results are expressed as fold changes of every treatment group relative to LV-ctr; $^*p < 0.05$ versus R201H. All numerical data are presented as mean ± SD. These data were from at least three independent experiments.

when a series of *GNAS* mutations were identified in McCune–Albright syndrome, FD and certain endocrine disorders [10–12,14–16,25]. However, the molecular mechanisms underlying how the *GNAS* mutations lead to the osteogenesis disorder of BMSCs remain unknown. Effective cell models, which can model the FD features *in vitro*, are needed greatly. In past research, three cell models have been used: (a) clonal FD-derived BMSCs with a GNAS mutation; (b) normal BMSCs treated with exogenous cAMP; and (c) normal BMSCs engineered to stably express mutated Gsα by lentivirus vector. Of these, clonal FD-derived BMSCs with *GNAS* mutations are undoubtedly the best cell model for FD research. However, these cells have been reported to not grow normally *in vitro*. This observation further supports Happle's hypothesis concerning the lethal nature of the mutation and that mutant cells can only survive when supported by normal cells [20,21,26]; additionally, the inability of 100% mutant cells to survive is probably due to the increased number of population doublings that would be needed to obtain enough cells for the experiments.

In the present study, we employed the other two *in vitro* cell models: LV-R201H BMSCs and cAMP-treated BMSCs, which model different aspects of FD pathogenesis. The former mimics the *GNAS* mutation that is the direct cause of FD and the latter mimics intracellular cAMP accumulation, which is one of the most important features of the FD phenotype. These two cell models each have some advantages respectively. The cAMP dose and treatment duration are easy to control, so the cAMP-treated BMSC model is suitable for investigations on signalling pathways. However, cAMP over-production does not contribute to all FD phenotypes and other signalling pathways activated by mutated *GNAS* are involved in the pathogenesis of FD [27]. Hence, the LV-R201H BMSC model is advantageous. By transducing normal BMSCs with lentivirus vectors, more consistent populations of cells can be better utilized to determine the level of the mutational load necessary to generate a lesion and to study changes in cellular metabolism by genomic and proteomic analyses. In this sense, *in vitro* investigation of FD pathogenesis requires the combination of these two cell models, which each offer certain advantages and can overcome each other's limitations to some extent.

Using these two cell models, we confirmed the involvement of the CREB–Smad6–Runx2 axis in the osteogenesis disorder of BMSCs with the FD phenotype. In 1975, DiGeorge [28] concluded an editorial by stating that MAS was 'a rare disorder, yes; an unimportant one, never'. However, the pathogenesis of MAS and FD has remained an open question and has not been defined in more stringent, mechanistic terms to date. In 1998, Olsen [26] also wrote an editorial about FD and raised obvious questions about the role of cAMP-dependent mechanisms in the differentiation of normal osteoblasts. He speculated that Runx2 might

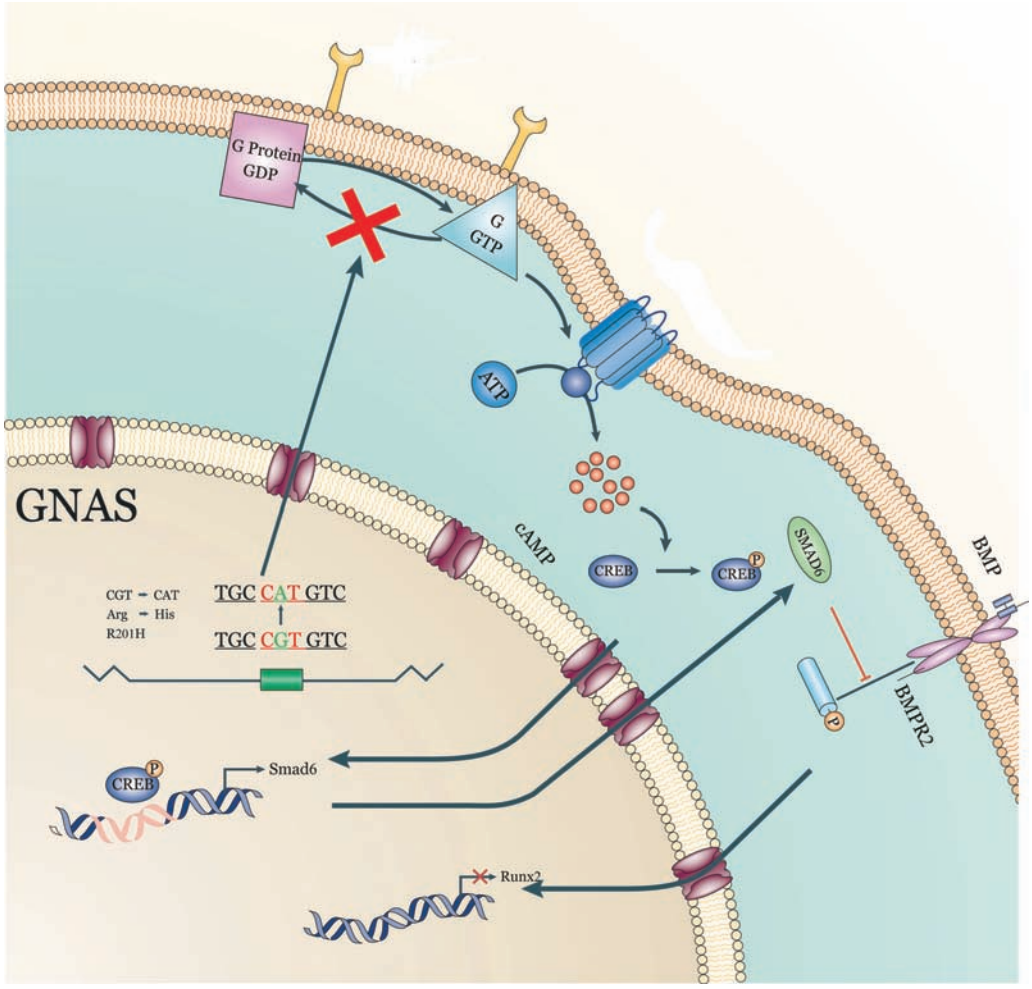

Figure 7. The CREB–Smad6–Runx2 axis in disordered osteogenesis by BMSCs in FD lesions. Substitution of His for Arg at position 201 in the *Gsα* subunit gene leads to the loss of GTPase activity and consequently to increased stimulation of adenylyl cyclase (AC) and over-production of cAMP. CREB is phosphorylated in response to over-production of cAMP, translocates into the nucleus and binds to the CRE of the Smad6 promoter to activate its transcription. Up-regulation of Smad6 inhibits the activation of Runx2 induced by BMP-2.

be a possible final target for the cAMP-dependent signalling pathway. The present study confirmed this speculation. Moreover, our results suggest that CREB and Smad6 are upstream of Runx2 and that the CREB–Smad6–Runx2 axis plays an essential role in the FD phenotype. Due to the lethal nature of clonal FD-derived BMSCs with GNAS mutations, we employed non-clonal FD-derived BMSCs to confirm the involvement of the CREB–Smad6–Runx2 axis in the impaired osteogenesis of FD BMSCs.

Some results from an elegant study by Piersanti *et al* [27] differed from those in the current study. Whereas there was no decrease in Runx2 in osteogenic differentiation conditions with or without IBMX in their LV-R201C cells, we observed Runx2 down-regulation in the current report. We think this difference is likely due to two potential reasons: (a) they used dexamethasone, ascorbic acid and β-glycerol phosphate, and we employed BMP-2, a potent activator of Runx2 expression, to induce BMSCs to undergo osteogenesis; and (b) it is known that lentivirus vectors randomly integrate into the genome of target cells. The copies and locations of inserts into the genome cannot be controlled concisely. Therefore, it is possible that lentivirus vector sequences inserted into the genome alter the expression profile of one or more gene(s) and affect biological functions. In that sense, results using lentivirus vectors must be prudently analysed. Thus, we employed non-clonal FD-derived BMSCs to confirm the involvement of the CREB–Smad6–Runx2 axis in the FD phenotype. In the current study, some differences, including mRNA expression of collagen I and *Smad6*, were observed between FD-derived BMSCs and LV-R201H BMSCs. We propose that these differences not only were due to the effect of lentivirus insertion into the genome of LV-R201H BMSCs but also resulted from the more profound complexity of FD-derived BMSCs compared to BMSCs engineered to stably express *GNAS* R201H *in vitro*.

There are many ways that stem cells could be utilized in the treatment of FD [6,29]. Given the fact that many patients with FD have unaffected bone, bone marrow from these bones could be isolated and expanded *ex vivo* to generate a population of BMSCs. These cells could then be used to repair an FD lesion through open surgery and transplantation of the cells along with an

appropriate scaffold. However, there are patients that do not have a reasonably accessible source of normal bone marrow and alternative methods must be utilized to obtain a population of normal BMSCs. In cases where only a mixed population of normal and mutant cells can be obtained, cloning of individual CFU-Fs and their progeny and subsequent genotyping could be used to generate a population of 100% normal BMSCs. In cases where the majority of cells are mutant, the use of virus vectors to silence mutated Gsα [27], over-express Runx2 and/or silence Smad6, as performed in the current study, may be used to generate cells that are amenable for use in bone regeneration.

In summary, our results suggest that the CREB–Smad6–Runx2 axis plays an essential role in the FD phenotype (Figure 7). This study provides useful insight into the molecular pathogenesis of FD and testing of novel therapies.

Acknowledgment

This study was supported by the National Natural Science Foundation of China (Grant No. 81000778), the Shanghai Science and Technology Development Fund (Grant No. 10410711100), the Scientific Research and Innovation of Shanghai Municipal Education Commission (Grant No. 11YZ46), the Shanghai Science Technology Development Fund (Grant No. 11XD 1403300) and the Key Disciplines of Shanghai Municipal Education Commission (Grant No. J50206).

Author contributions

Q-MF and BY conceived and carried out experiments; Z-YB, W-TX and BT carried out experiments and analysed data; KD, GL and T-TT conceived experiments, analysed data and wrote the paper.

References

1. Bianco P, Riminucci M, Majolagbe A, *et al*. Mutations of the *GNAS1* gene, stromal cell dysfunction, and osteomalacic changes in non-McCune–Albright fibrous dysplasia of bone. *J Bone Miner Res* 2000; **15**: 120–128.
2. Albright FBA, Hampton AO, Smith P. Syndrome characterized by osteitis fibrosa disseminata, areas of pigmentation and endocrine dysfunction with precocious puberty in females. *N Engl J Med* 1937; **216**: 727–746.
3. Faivre L, Nivelon-Chevallier A, Kottler ML, *et al*. Mazabraud syndrome in two patients: clinical overlap with McCune–Albright syndrome. *Am J Med Genet* 2001; **99**: 132–136.
4. Zoccali C, Teori G, Prencipe U, *et al*. Mazabraud's syndrome: a new case and review of the literature. *Int Orthop* 2009; **33**: 605–610.
5. Kuznetsov SA, Cherman N, Riminucci M, *et al*. Age-dependent demise of *GNAS*-mutated skeletal stem cells and 'normalization' of fibrous dysplasia of bone. *J Bone Miner Res* 2008; **23**: 1731–1740.
6. Robey PG, Kuznetsov S, Riminucci M, *et al*. The role of stem cells in fibrous dysplasia of bone and the McCune–Albright syndrome. *Pediatr Endocrinol Rev* 2007; **4**(suppl 4): 386–394.
7. Danon M, Crawford JD. The McCune–Albright syndrome. *Ergeb Inn Med Kinderheilkd* 1987; **55**: 81–115.
8. Greco MA, Steiner GC. Ultrastructure of fibrous dysplasia of bone: a study of its fibrous, osseous, and cartilaginous components. *Ultrastruct Pathol* 1986; **10**: 55–66.
9. Kransdorf MJ, Moser RP, Jr., Gilkey FW. Fibrous dysplasia. *Radiographics* 1990; **10**: 519–537.
10. Schwindinger WF, Francomano CA, Levine MA. Identification of a mutation in the gene encoding the α-subunit of the stimulatory G protein of adenylyl cyclase in McCune–Albright syndrome. *Proc Natl Acad Sci USA* 1992; **89**: 5152–5156.
11. Shenker A, Weinstein LS, Moran A, *et al*. Severe endocrine and nonendocrine manifestations of the McCune–Albright syndrome associated with activating mutations of stimulatory G protein GS. *J Pediatr* 1993; **123**: 509–518.
12. Weinstein LS, Shenker A, Gejman PV, *et al*. Activating mutations of the stimulatory G protein in the McCune–Albright syndrome. *N Engl J Med* 1991; **325**: 1688–1695.
13. Candeliere GA, Glorieux FH, Prud'homme J, *et al*. Increased expression of the *c-fos* proto-oncogene in bone from patients with fibrous dysplasia. *N Engl J Med* 1995; **332**: 1546–1551.
14. Malchoff CD, Reardon G, MacGillivray DC, *et al*. An unusual presentation of McCune–Albright syndrome confirmed by an activating mutation of the Gs α-subunit from a bone lesion. *J Clin Endocrinol Metab* 1994; **78**: 803–806.
15. Marie PJ, de Pollak C, Chanson P, *et al*. Increased proliferation of osteoblastic cells expressing the activating Gsα mutation in monostotic and polyostotic fibrous dysplasia. *Am J Pathol* 1997; **150**: 1059–1069.
16. Shenker A, Weinstein LS, Sweet DE, *et al*. An activating Gsα mutation is present in fibrous dysplasia of bone in the McCune–Albright syndrome. *J Clin Endocrinol Metab* 1994; **79**: 750–755.
17. Yamamoto T, Ozono K, Kasayama S, *et al*. Increased IL-6-production by cells isolated from the fibrous bone dysplasia tissues in patients with McCune–Albright syndrome. *J Clin Invest* 1996; **98**: 30–35.
18. Alman BA, Greel DA, Wolfe HJ. Activating mutations of Gs protein in monostotic fibrous lesions of bone. *J Orthop Res* 1996; **14**: 311–315.
19. Shenker A, Chanson P, Weinstein LS, *et al*. Osteoblastic cells derived from isolated lesions of fibrous dysplasia contain activating somatic mutations of the Gsα gene. *Hum Mol Genet* 1995; **4**: 1675–1676.
20. Bianco P, Robey PG. An animal model of fibrous dysplasia. *Mol Med Today* 1999; **5**: 322–323.
21. Bianco P, Kuznetsov SA, Riminucci M, *et al*. Reproduction of human fibrous dysplasia of bone in immunocompromised mice by transplanted mosaics of normal and Gsα-mutated skeletal progenitor cells. *J Clin Invest* 1998; **101**: 1737–1744.
22. Laverriere JN, Muller M, Buisson N, *et al*. Differential implication of deoxyribonucleic acid methylation in rat prolactin and rat growth hormone gene expressions: a comparison between rat pituitary cell strains. *Endocrinology* 1986; **118**: 198–206.
23. Matsubara T, Kida K, Yamaguchi A, *et al*. BMP2 regulates Osterix through Msx2 and Runx2 during osteoblast differentiation. *J Biol Chem* 2008; **283**: 29119–29125.
24. Massague J, Seoane J, Wotton D. Smad transcription factors. *Genes Dev* 2005; **19**: 2783–2810.
25. Landis CA, Masters SB, Spada A, *et al*. GTPase inhibiting mutations activate the α-chain of Gs and stimulate adenylyl cyclase in human pituitary tumours. *Nature* 1989; **340**: 692–696.
26. Olsen BR. 'A rare disorder, yes; an unimportant one, never'. *J Clin Invest* 1998; **101**: 1545–1546.

27. Piersanti S, Remoli C, Saggio I, *et al*. Transfer, analysis, and reversion of the fibrous dysplasia cellular phenotype in human skeletal progenitors. *J Bone Miner Res* 2010; **25**: 1103–1116.
28. Di George AM. Editorial: Albright syndrome: is it coming of age? *J Pediatr* 1975; **87**: 1018–1020.
29. Bianco P, Robey PG. Stem cells in tissue engineering. *Nature* 2001; **414**: 118–121.

SUPPORTING INFORMATION ON THE INTERNET

The following supporting information may be found in the online version of this article:

Figure S1. Normal BMSCs were exposed to 200, 300 and 500 ng/ml BMP-2 *in vitro* culture and 1 week later ALP staining and quantification assay were performed. Futher, normal BMSCs were exposed to 200 ng/ml BMP-2 in combination with 0.5, 1 and 2 mM cAMP and 1 week later ALP staining and quantification assay were performed.

Figure S2. After isolation from FD lesion and culture *in vitro*, FD-derived BMSCs were injected into the bone marrow cavitry of femur of nude mice. Eight weeks later, X-ray imaging, HE staining and allele-specific PCR were performed.

Figure S3. Bone marrow stromal cells (BMSCs) were isolated from FD lesions and plated in 10 cm culture dishes at very low density.

Figure S4. In the current study, we screened three key transcription factors in osteogenesis, *Runx2, Msx2* and *Osx*, by exposing normal BMSCs to BMP-2 and excess cAMP and quantifying their mRNA abundance.

Figure S5. Having observed the down-regulation of Runx2 in response to excess cAMP, we employed adenovirus vectors to over-express Runx2, to investigate its potential role in the inhibition of osteogenesis by excess cAMP.

Table S1. Primer sequences used for RT–PCR.